Fitoterapia 137 (2019) 104255

Contents lists available at ScienceDirect

Fitoterapia

journal homepage: www.elsevier.com/locate/fitote

The biflavonoids as protein tyrosine phosphatase 1B inhibitors from *Selaginella uncinata* and their antihyperglycemic action

Jinfang Xu[a], Lijun Yang[a], Rong Wang[a], Ke Zeng[a], Boyi Fan[b], Zhengbao Zhao[a,*]

[a] School of Pharmaceutical Science, Shanxi Medical University, 56 Xinjian Road, Taiyuan 030001, People's Republic of China
[b] School of Pharmacy, Nantong University, 19 Qixiu Road, Nantong, 226001 Jiangsu Province, People's Republic of China

ARTICLE INFO

Keywords:
Selaginella uncinate
Biflavonoids
Protein tyrosine phosphatase 1B
Molecular docking
Glucose uptake
Insulin resistance

ABSTRACT

Nine biflavonoids (**1–9**) were isolated from ethanolic extract of *Selaginella uncinata* (Desv.) Spring. Their structures were determined by spectra analysis. Compounds **1–9** were classified into four types according to the connection styles of the two flavonoid parts. Among them, **1** was elucidated as a new compound, while **4** was one with a new configuration. All isolates exhibited inhibitory activities against protein tyrosine phosphatase 1B (PTP1B) in an enzyme assay with IC_{50} values ranging from 4.6 to 16.1 μM, and the relationship between the structures and activities was discussed. Docking simulations of these compounds demonstrated they had tight binding capacities towards the allosteric site of PTP1B. Additionally, the glucose uptake activities of **1–9** were evaluated in insulin-resistant HepG2 cells, while the effect of **1** on the activation of IRS-1/PI3K/Akt pathway was revealed by Western Blot analysis.

1. Introduction

Diabetes mellitus is a metabolic disease characterized by high blood glucose levels associated with a series of chronic complications such as cardiovascular disease and pathological changes of retina and kidney [1]. The International Diabetes Federation (IDF) in 2015 reported that over 415 million individuals worldwide suffered from diabetes, and this number was estimated to increase to 642 million by 2040 [2]. More than 90% of all diabetes cases belong to type 2 diabetes (T2DM). Insulin resistance, a key feature of T2DM, reflect in decreased insulin sensitivity of major organs such as muscle and liver, leading to defect in muscle glucose uptake and overproduction of glucose in liver [3,4]. Therefore, discovery of new anti-diabetic drugs acting as insulin mimics and/or insulin sensitizers has become a common practice by both the pharmaceutical industry and academia nowadays.

Protein tyrosine phosphatase 1B (PTP1B) enzyme, a member of the protein tyrosine phosphatase family, has been confirmed to lead to insulin resistance by blocking intracellular insulin signaling pathway. In brief, metabolic insulin signal transduction occurs through activation of insulin receptor (IR) as well as the downstream insulin receptor substrate-1 (IRS-1). This is followed by phosphorylation of phosphatidylinositol-3 kinase (PI3K) and protein kinase B (PKB; also known as AKT). The activated AKT subsequently boosts GLUT4 translocation to the membrane from inner vesicles and finally provokes glucose uptake [5]. PTP1B is involved in this process as a key negative regulator of IR and IRS, leading to the attenuation of the insulin signal. Therefore, the inhibition of the activity of PTP1B can affect glucose uptake and prevent the insulin resistance observed in T2DM [6].

Nature continues to provide a rich source of lead compounds in the development of new antidiabetic agents [7,8]. As we known, metformin, originally derived from a natural product galegine, is used as the first-line drug for T2DM treatment [9]. Biflavonoids are naturally occurring flavonoid-flavonoid dimers connected by C—C or C-O-C bonds with varied chemical structures. Their biological activities, such as PTP1B inhibitory and antihyperglycemic effects, have attracted great attentions [10]. Unlike their monomeric constituents, biflavonoids exist in nature restricted to some species, such as *Selaginella* and *Ginkgo biloba* [11]. *Selaginella uncinata* (Desv.) Spring, a traditional Chinese plant belongs to the *Selaginella* genus, is widely distributed in Southeast Asian countries. It has been used for the treatment of pneumonia, pulmonary tuberculosis, jaundice, dysentery and edema [12]. However, the biological studies of *S. uncinata* targeting diabetes are limited. In our present investigation to find new antidiabetic agents from medicinal plants, the chemical composition of *S. uncinata* was investigated. Nine biflavonoids (**1–9**) were isolated from the methanol extract of *S. uncinate* (Fig. 1). Compound **1** was elucidated as a new biflavonoid, and **4** possessed a new configuration. All the isolates were evaluated for the inhibitory effects on PTP1B enzyme, and their binding modes were

* Corresponding author.
E-mail addresses: xjf.0358@163.com (J. Xu), fanboyi@ntu.edu.cn (B. Fan), zhengbao_z@sxmu.edu.cn (Z. Zhao).

https://doi.org/10.1016/j.fitote.2019.104255
Received 8 May 2019; Received in revised form 25 June 2019; Accepted 1 July 2019
Available online 02 July 2019

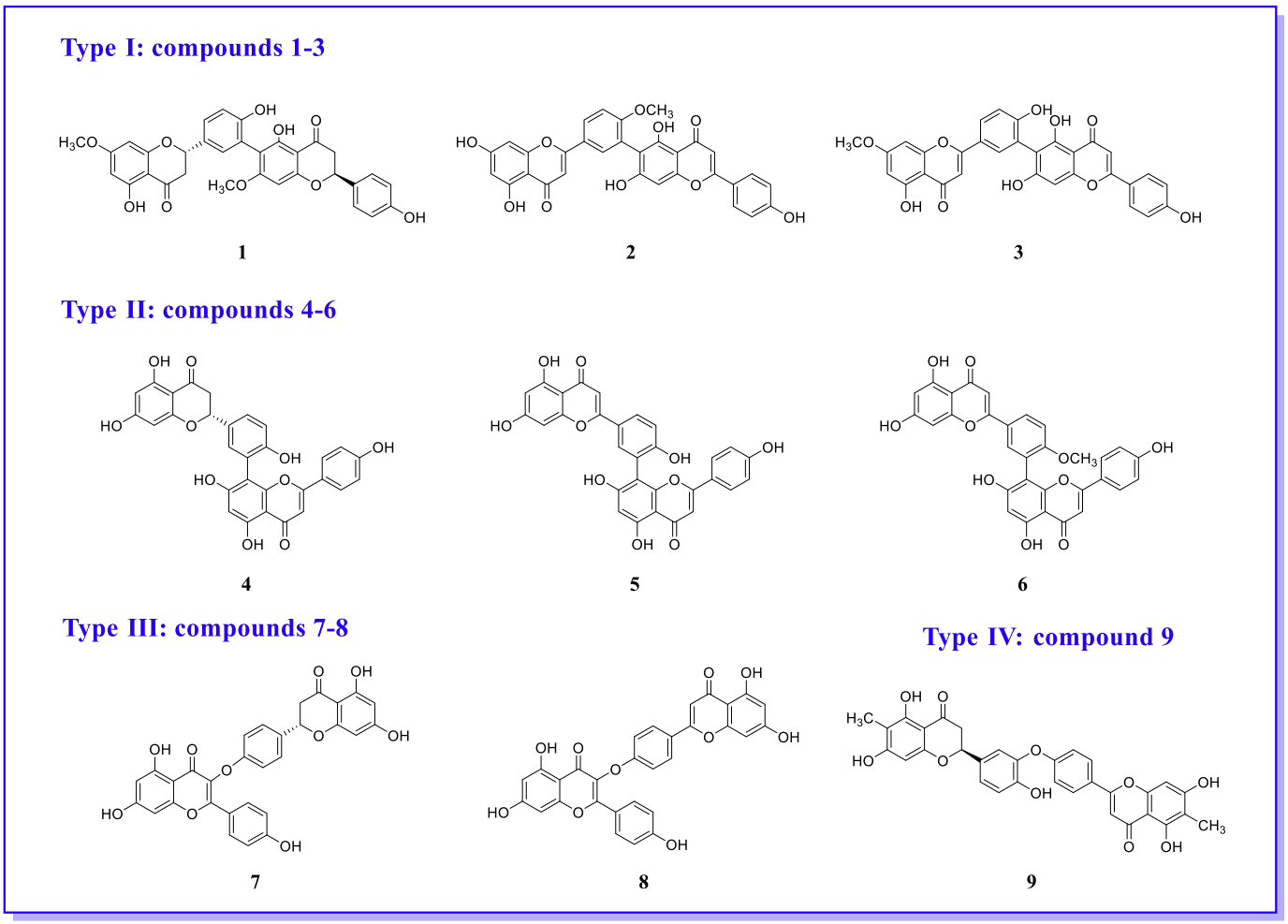

Fig. 1. Chemical structures of isolated compounds (**1**–**9**) from *S. uncinata*.

studied by molecular docking. Furthermore, their stimulatory effects on glucose uptake in HepG2 cells were tested. Compound **1**, which was found to possess the most potent stimulatory effect, was additionally tested for its effect on the activities of the IRS-1/PI3K/Akt signaling pathway in a cell-based assay.

2. Experimental

2.1. General experimental procedures

The UV spectra were obtained on a Hitachi U-3900 spectrophotometer. A Nicolet Magna-IR iS5 spectrometer was used to record the IR data. CD spectra were determined on a BioLogic MOS-500 spectrometer. NMR spectra were acquired using a Bruker instrument at 400 MHz (^{1}H) and 101 MHz (^{13}C) with Me_4Si as an internal standard. High resolution mass spectra (HRMS) were recorded on an Agilent 1100 LC-MSD-Trp-SL using electrospray ionization (ESI). Semipreparative HPLC was performed on a K-2501 system (Lumiere, Tech. Ltd. China) equipped with an MP-C18 column (250 mm × 21.2 mm, 10 μm, Venusil Corporation, China), using a flow rate of 3.0 mL/min at a column temperature of 25 °C.

2.2. Plant material

The dried herbs of *S. uncinata* were collected in March 2017 from Bozhou, Anhui, People's Republic of China, and were identified by Professor Bai Yune, Department of Medicinal Plants, Shanxi Medical University. Voucher specimens (SU-20170302) were deposited at the Chinese Medicine Herbarium, Shanxi Medical University.

2.3. Extraction and isolation

The air-dried whole herbs of *S. uncinata* (5.0 kg) were extracted three times with 80% EtOH (3 × 15 L, 2.5 h each) under reflux conditions. The solution was evaporated under reduced pressure to obtain a residue (956.0 g). The residue was dissolved in water, and then partitioned with petroleum ether, ethyl acetate, and n-butyl alcohol, successively. The ethyl acetate soluble fraction (83.0 g) was subjected to silica gel column chromatography (CC) eluted with dichloromethane-methanol (50:1, 20:1, 8:1, 4:1) to afford six fractions (Fr. A-F). Fr. B (8.6 g) was decolored by MCI gel CC (CH_3OH/H_2O, 90:10, *v/v*), followed by ODS CC (CH_3OH/H_2O, 40: 60, *v/v*) to obtain **1** (50.1 mg). Fr. C (17.4 g) was decolored on MCI-gel CC eluted with aqueous CH_3OH/H_2O (90:10) and then separated over an ODS CC (CH_3OH/H_2O, 30:70 to 80:20, *v/v*) to afford two major subfractions Fr. C-1 and Fr. C-2. Furthermore, Fr. C-1 was separated by Sephadex LH-20 CC (CH_3OH) and semipreparative HPLC eluted with CH_3OH/H_2O (70:30, *v/v*) to obtain **4** (67.2 mg). Fr. C-2 was subjected to Sephadex LH-20 CC (CH_3OH) followed by semipreparative HPLC eluted with CH_3OH/H_2O (55:45, *v/v*) to produce **9** (44.3 mg). Fr. D (7.1 g) was chromatographed on MCI-gel CC eluted with aqueous CH_3OH to afford Fr. D-1 and Fr. D-2. Fr. D-1 was purified by Sephadex LH-20 (CH_3OH) to obtain **7** (20.2 mg). Fr. D-2 was separated by ODS CC (CH_3OH/H_2O, 60:40, *v/v*) followed by semipreparative HPLC eluted with CH_3OH/H_2O (52:48, *v/*

Table 1
^{1}H NMR (400 MHz) and ^{13}C NMR (101 MHz) data of **1** and **4** in DMSO-d_6.

1			**4**		
No.	δ_H (*J* in Hz)	δ_C	No.	δ_H (*J* in Hz)	δ_C
2	5.49 (dd, *J* = 12.9, 2.6 Hz, 1H)	79.3	2	5.66 (dd, *J* = 1.6, 13.2 Hz, 1H)	78.7
3	2.73 (dd, *J* = 16.4, 2.6 Hz, 1H) 3.38(dd, *J* = 16.4, 12.9 Hz, 1H)	42.0	3	2.84 (dd, *J* = 16.0, 1.6 Hz, 1H) 3.51(dd, *J* = 13.2, 16.0 Hz,1H)	42.5
4		197.0	4		196.4
5		163.3	5		163.6
6	6.08 (d, *J* = 1.8 Hz, 1H)	94.7	6	6.05 (d, *J* = 1.8 Hz, 1H)	95.9
7		167.5	7		166.8
8	6.12 (d, *J* = 1.8 Hz, 1H)	93.8	8	6.05 (d, *J* = 1.8 Hz, 1H)	95.1
9		163.0	9		163.2
10		102.7	10		101.8
1′		128.2	1′		129.7
2′	7.14 (d, *J* = 1.7 Hz, 1H)	131.5	2′	7.56 (d, *J* = 1.7, 1H)	131.6
3′		119.6	3′		119.3
4′		156.2	4′		156.2
5′	6.90 (d, *J* = 8.3 Hz, 1H)	115.4	5′	7.18 (d, *J* = 8.4 Hz, 1H)	115.8
6′	7.31 (dd, *J* = 8.3, 1.7 Hz, 1H)	127.3	6′	7.56 (dd, *J* = 8.4, 1.7, 1H)	127.9
2″	5.54 (dd, *J* = 12.9, 2.6 Hz, 1H)	78.8	2″		161.2
3″	2.77 (dd, *J* = 16.4, 2.6 Hz, 1H) 3.35 (dd, *J* = 16.4, 12.9 Hz, 1H)	42.0	3″	6.93 (s, 1H)	102.5
4″		197.1	4″		182.2
5″		159.8	5″		160.3
6″		107.3	6″	6.53 (s, 1H)	98.8
7″		165.3	7″		162.6
8″	6.30 (s, 1H)	91.5	8″		105.0
9″		162.7	9″		154.5
10″		102.4	10″		103.5
1‴		128.8	1‴		121.5
2‴/6‴	7.37 (d, *J* = 8.2 Hz, 2H)	128.5	2‴/6‴	7.75 (d, *J* = 8.5 Hz, 2H)	128.4
3‴/5‴	6.83 (d, *J* = 8.2 Hz, 2H)	115.2	3‴/5‴	6.95 (d, *J* = 8.5 Hz, 2H)	115.9
4‴		157.9	4‴		163.6
7-OMe	3.78 (s, 3H)	55.9			
7″-OMe	3.71 (s, 3H)	56.2			
OH-4′	9.34 (s, 1H)				
OH-5	12.14 (s, 1H)			12.32 (s, 1H)	
OH-4‴	9.65 (s, 1H)				
OH-5″	12.18 (s, 1H)			13.24 (s, 1H)	

v) to obtain **2** (10.6 mg), **3** (6.8 mg), **6** (13.6 mg) and **8** (58.5 mg). Fr. E (23.5 g) were subjected to a MCI-gel CC (MeOH isocratic elution) and silica gel column chromatography (CH_2Cl_2/CH_3OH, 12:1, *v/v*) to yield **5** (24.9 mg).

2.3.1. Uncinatabiflavone C 7-methyl ether (1)

Yellow gum; UV (CH_3OH) λ_{max} (log ε): 281 (4.31), 332 (3.78) nm; CD (MeOH, c = 49.1 μmol/L), λ_{max} (Δε) 330.0 (+4.56), 285.0 (−5.04); IR (KBr) ν_{max} 2919, 2848, 1630, 1573, 1517, 1447, 1364, 1340, 1279, 1202, 1155, 1107, 1088, 1022, 997, 819, 710 cm^{-1}; ^{1}H and ^{13}C NMR data see Table 1; HRESIMS *m/z* 569.1445 [M – H] $^{-}$ (calcd for $C_{32}H_{25}O_{10}$, 569.1526).

2.3.2. (2R) 2, 3-dihydroamentoflavone (4)

Yellow gum; UV (MeOH) λ_{max} (log ε) 264 (4.23), 324 (4.01); CD (MeOH, *c* = 44.9 μmol/L) λ_{max} (Δε) 329.0 (+2.33), 287.0 (−10.99); IR ν_{max} (KBr) 2915, 2847, 1639, 1607, 1573, 1507, 1421, 1364, 1281, 1240, 1173, 1108, 1021, 992, 822 cm^{-1}; ^{1}H and ^{13}C NMR data see Table 1; HRESIMS *m/z* 539.0975 [M–H]$^{-}$ (calcd for $C_{30}H_{20}O_{10}$, 539.1056).

2.4. PTP1B inhibitory assay

PTP1B inhibition assays of the isolated compounds were carried out in a 96-well microplate using *p*-nitrophenyl phosphate (*p*-NPP) as the substrate according to previously published protocol with some modifications [13]. To each well, 20 μL PTP1B enzyme (1 μg/mL) dissolved in a buffer (pH 7.0) containing HEPES (25 mM), NaCl (150 mM), EDTA (1 mM) and DTT (3 mM) was added with or without test compounds (final concentration 50 mM, dissolved in 10% DMSO). The plate was pre-incubated at 37 °C for 15 min, and then implemented with 40 μL of *p*-NPP (3 mM). The reaction was terminated with 10 M NaOH. The amount of *p*-nitrophenolate, which was produced by enzymatic dephosphorylation of *p*-NPP, was measured at 405 nm using a microplate spectrophotometer. The results were expressed as the percentage of inhibition of PTP1B activity. Ursolic acid was used as positive control.

2.5. Molecular docking simulation in PTP1B inhibition

The molecular docking simulations were performed with AutoDock Tools-1.5.6 software to estimate the conformation of the protein–ligand complex. The 3D crystal structure of PTP1B (PDB ID: 1T49) was obtained from the RCSB Protein Data Bank. The removement of water molecules and binding inhibitor from the structure was performed using Sybyl-X 2.0 software. The structure of the compounds **1–9** were mapped and converted to 3D conformation using Chem3D Pro 14.0 software. After protonated and energy minimized, these small molecule ligands were introduced into AutoDock-1.5.6 software. Docking calculations were then performed between the minimized ligand through a cube (dimensions 24 × 24 × 24 Å, grid spacing 0.375 Å) located in the geometric center (coordinates 53.6, 35.7, 20.2) of the reported binding pocket present in the PTP1B receptor. The predicted protein–ligand complexes were optimized and ranked according to the docking score, which indicated the binding free energy and affinity.

2.6. Induction of insulin-resistant HepG2 cells

Human hepatoma (HepG2) cells were cultured in RPMI-1640 supplemented with 10% fetal bovine serum and 1% penicillin-streptomycin solution. The cells were maintained at 37 °C in a humidified atmosphere of 5% CO_2. Insulin resistance was induced in HepG2 cells following a previously described protocol with minor modifications [14]. Serum-free medium was used to substitute the original medium for 24 h after cells had been seeded. After pretreatment with serum-free medium containing normal (5.5 mM) or high (30 mM) concentrations of D-glucose for 24 h, the cells were cultured in 100 mg/L insulin for another 24 h, and then cultured for 2 h in serum medium and harvested for the following assays.

2.7. Glucose uptake and cell viability assay

The glucose uptake rate was measured using the glucose assay kit (glucose oxidase method) according to the published procedure [15]. The insulin-resistant HepG2 cells in the logarithmic growth phase were plated into 96-well plates at 5000/well with some wells left blank, and cultured in serum-free, high-glucose medium with or without tested compounds and metformin (5, 10, 20 μM) for 24 h. Then, 40 μL of the culture solution was used to detect the residual glucose content using a glucose kit. Glucose consumption (GC) = blank group cell glucose content – drug group cell glucose content.

3-(4,5-dimethylthiazol-2-yl)-2,5-diphenyltetrazoliumbromide (MTT) was used for the cell viability assay [16]. After 36 h of cell culture, 10 μL of MTT was added to each well and cultured at 37 °C for 4 h. The medium was aspirated and 150 μL of DMSO was added for

10 min. The absorbance of each well was measured at 568 nm by a microplate reader to obtain MTT results. The MTT results were used to normalize the glucose utilization results. Glucose consumption due to the cell proliferation can be deducted by calculating the ratio of the GC and MTT (GC/MTT).

2.8. Western blotting

The expression levels of each protein were analyzed by western blotting. Insulin-resistant HepG2 cells were cultured in 6-well plates treated with 2.5, 5.0, 10.0 μM solutions of compound **1**, and were washed with ice-cold PBS and lysed with lysis buffer. The proteins were transferred to a PVDF membrane and incubated with primary antibody, followed by secondary antibody. The positive bands in the blot were detected by chemiluminescence. The expression level of GAPDH was used as an internal standard control.

2.9. Statistical analyses

All data are expressed as the mean ± the standard deviation (SD) of three independent experiments. GraphPad Prism software (GraphPad, San Diego, CA, USA) were used for graphic representation and statistical analysis. Values of $p < 0.05$ were considered to be statistically significant.

3. Results and discussion

3.1. Isolation and structural elucidation of compounds

Compound **1** was obtained as a yellow gum. Its molecular formula was determined to be $C_{32}H_{26}O_{10}$ base on the ion peak at *m/z* 569.1445 $[M–H]^-$ (calcd 569.1526) in the HRESIMS. The UV spectrum showed the maximum absorption band I at 332 nm (log ε 3.78) and band II at 281 nm (log ε 4.31), which, in combination with the positive result for the Mg-HCl reaction, revealed that **1** was a flavonoid compound. The IR spectrum indicated absorption bands for hydroxy group (2919 cm^{-1}), chelated carbonyl (1630 cm^{-1}), and aromatic rings (1573 and 1447 cm^{-1}). Analysis of the ^1H NMR and ^{13}C NMR (Table 1) suggested that **1** should be a biflavonoid consisting of two flavanone units, as indicated by the characteristic resonances of two nonconjugated carbonyls at δ_C 197.0 (C-4) and 197.1 (C-4″), as well as six aliphatic resonances at δ_H 5.49 (dd, J = 12.9, 2.6 Hz, H-2), 2.73 (dd, J = 16.4, 2.6 Hz, H-3), 3.38(dd, J = 16.4, 12.9 Hz, H-3), 5.54 (dd, J = 12.9, 2.6 Hz, H-2″), 2.77 (dd, J = 16.4, 2.6 Hz, H-3″), and 3.35 (dd, J = 16.4, 12.9 Hz, H-3″). Two chelated OH groups at δ_H 12.14 (5-OH) and 12.18 (5″-OH), and two methoxy groups at δ_H 3.78 (s, 3H) and 3.71 (s, 3H) could also be found in the ^1H NMR spectrum. A set of *meta*-coupled doublets at δ_H 6.12 (1H, d, J = 1.8 Hz) and 6.08 (1H, d, J = 1.8 Hz) were assigned to be H-6 and H-8 of ring I-A. In addition, an ABM coupling system, with signals at δ_H 7.31 (1H, dd, J = 8.3, 1.7 Hz, H-6′), 7.14 (1H, d, J = 1.7, H-2′), and 6.90 (1H, d, J = 8.3, H-5′), indicating that C-3′ might be the position of linkage of the two flavanone units. The doublets at δ_H 7.37 (d, J = 8.2 Hz, H-2‴, H-6‴) and 6.83 (d, J = 8.2 Hz, H-3‴, H-5‴) could be assigned to the A_2B_2 spin system, which suggested that the ring II-B was *para*-substituted.

In the HMBC spectrum (Fig. 2), the correlations of H-2′ (δ_H 7.14) to C-2 (δ_C 79.3) and C-6″(δ_C 107.3), and 5″-OH (δ_H 12.18) to C-10″ (102.4), C-3′ (δ_C 119.6) and C-6″(δ_C 107.3), indicated that the linkage position of the units I and II was between C-3′ and C-6″, corresponding to the robustaflavone series. The methoxy groups were deduced to be located at C-7 and C-7″, respectively, on the basis of the HMBC cross-peaks from OCH_3 (δ_H 3.78) to C-7 (δ_C 167.5) and from OCH_3 (δ_H 3.71) to C-7″ (δ_C 165.3). All the other chemical shifts of carbons connected with protons were confirmed using the 2D NMR experiment. The ^{13}C NMR data of **1** showed many similarities to those of a known compound uncinatabiflavone C, except for the obvious changes at C-6, C-7, and C-8, indicating that C-7 was methoxylated [17]. The CD spectrum of **1** (see Supplementary data) showed a positive Cotton effect at 330 nm ($n \rightarrow \pi^*$ transition) and a negative Cotton effect at 285 nm ($\pi \rightarrow \pi^*$ transition). Therefore, the C-2 and C-2″ were both assigned as *S* configurated [18]. Compound **1** was identified as a new compound, named uncinatabiflavone C 7-methyl ether.

Compound **4** was obtained as a yellow gum, and the molecular formula of $C_{30}H_{20}O_{10}$ was determined by HRESIMS *m/z* at 539.0975 $[M–H]^-$ (calcd 539.1056). The UV spectrum was typical of biflavonoids, with a maximum at 264 nm (log ε 4.32), followed by a shoulder at 324 nm (log ε 4.01). The IR spectrum exhibited absorption bands at 2915, 1639, 1573, 1421 cm^{-1}, indicating the presence of hydroxyl, chelated carbonyl, and aromatic ring functionalities. The ^1H NMR and ^{13}C NMR (Table 1) of **4** was the same as that of 2, 3-dihydroamentoflavone, a known compound previously reported [19–21]. However, the CD spectrum of **4** showed cotton effects with a positive sign ($\pi \rightarrow \pi^*$ transition) at 288 nm and a negative sign ($n \rightarrow \pi^*$ transition) at 323 nm (see Supplementary data), indicating a 2*R* configuration, which is rare in natural biflavonoids and opposite to that of the reported one [18,19]. Thus, **4** was identified as (2*R*) 2, 3-dihydroamentoflavone, a compound with a new configuration.

By analysis of the spectroscopic data and in comparison with the literatures, the chemical structures of seven known compounds were identified as, robustaflavone 4′-methyl ether (**2**) [22], robustaflavone 7-methyl ether (**3**) [23], amentoflavone (**5**) [24], bilobetin (**6**) [25], (2″*S*) chrysocauloflavone I (**7**) [26], delicaflavone (**8**) [27], (2*S*) 2,3-dihydro-5,5″,7,7″,4′-pentahydroxy-6,6″-dimethyl-[3′-O-4‴]-biflavone (**9**) [28]. These biflavonoids were classified into four types according to the connection styles of the two flavonoid parts (Fig. 1) [23]: type I, robustaflavone-type biflavonoids in which the two flavonoids were linked by C3′-C6″ (compounds **1–3**); type II, amentoflavone-type biflavonoids in which the two parts were connected by C3′-C8″ (compounds **4–6**); type III, delicaflavone-type biflavonoids in which the two parts were are not a C—C bond but a C3-O-C4‴ bond (compounds **7** and **8**); and type IV, a biflavonoid with C3′-O-C4‴ connection (compound **9**).

3.2. PTP1B inhibitory activity

All the isolated compounds were tested for their inhibitory activities against PTP1B using an in vitro assay. Ursolic acid, a known PTP1B inhibitor, was used as the positive control. Compounds **1–9** inhibited PTP1B activity in a dose-dependent manner with IC_{50} values ranging from 4.6 ± 0.5 to 16.1 ± 0.5 μM. Comparing with ursolic acid (IC_{50} = 3.1 ± 0.4 μM), compound **9** was the most potent with IC_{50} values of 4.6 ± 0.5 μM. As second potent inhibitors, compounds **7** and **8** exhibited IC_{50} values of 5.5 ± 0.7 μM and 6.2 ± 0.5 μM, respectively, followed by **1**, **2** and **3** presenting IC_{50} values of 7.7 ± 0.3 μM, 9.2 ± 0.4 μM, and 9.8 ± 0.5 μM, respectively. Compounds **4**, **5** and **6** showed relatively weak PTP1B inhibition with IC_{50} values of 16.1 ± 0.5 μM, 10.6 ± 0.3 μM, and 14.6 ± 0.80 μM, respectively. The relationship between certain structural features of **1–9** and their PTP1B inhibitory activities was observed. It appeared that all the above biflavonoids were active. The type III (**7** and **8**) and type IV biflavonoids (**9**), with the C-O-C linkage axis, possessed stronger inhibitory effects on PTP1B activity than other molecules. Among them, the activity of **9** was the strongest one. On the contrary, the amentoflavone-type biflavonoids (**4–6**) with the C3′-C8″ connection were less active. Thus, it is suggested that the linkage between two flavonoid skeletons may influence the inhibitory effect on PTP1B enzyme. Additionally, the presence of the less polar substituents, both 6- and 6″-methyl groups in compound **9**, also contribute to increase the ability to inhibit PTP1B. These conclusions were in accordance with that of the previous studies [29,30].

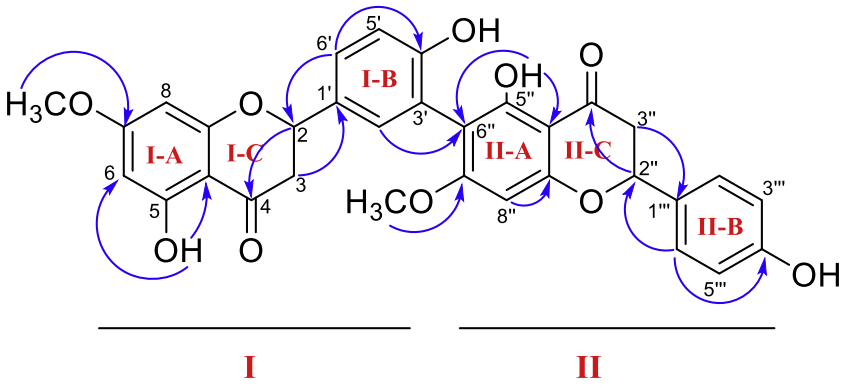

Fig. 2. The structure and key HMBC correlations of **1**.

Table 2
Binding site residues and docking scores of compounds **1–9** in PTP1B using AutoDock Tools-1.5.6.

Compounds	Binding Energy	Number of H-Bond	H-Bond interacting residues	Ligand binding sites
Inhibitor	−9.07	1	Glu276	Leu192, Asn193, Phe196, Lys279,Phe280, Ile281
1	−7.16	3	Ser187, Ser190, Tyr152,	Ser187, Ala189, Leu192, Phe196, Asn193
2	−6.47	1	Lys197	Ala189, Leu192, Asn193, Phe196, Glu200, Glu276, Phe280
3	−6.02	0	–	Ser151, Tyr152, Ala189, Leu192, Asn193, Phe196, Glu200, Phe280
4	−7.44	0	–	Leu192, Asn193, Phe196, Glu276, Gly277, Phe280, Ile281
5	−8.88	5	Lys150, Ser151, Tyr152, Lys197	Tyr153, Ala189, Leu192, Asn193, Phe196, Glu200
6	−8.42	1	Tyr152	Lys150, Ser151, Tyr153, Ala189, Leu192, Asn193, Phe196, Lys197, Glu200
7	−7.72	2	Ser151	Lys150, Ala189, Asn193, Phe196, Phe280
8	−7.63	3	Ser151, Lys277	Lys150, Tyr152, Tyr153, Ala189, Asn193, Phe196, Phe280
9	−9.49	1	Asn193	Ser151, Tyr152, Tyr153, Ser190, Leu192, Phe196, Gly277
Ursolic acid	−7.25	1	Tyr152	Ser151, Tyr153, Ala189, Asn193, Phe280

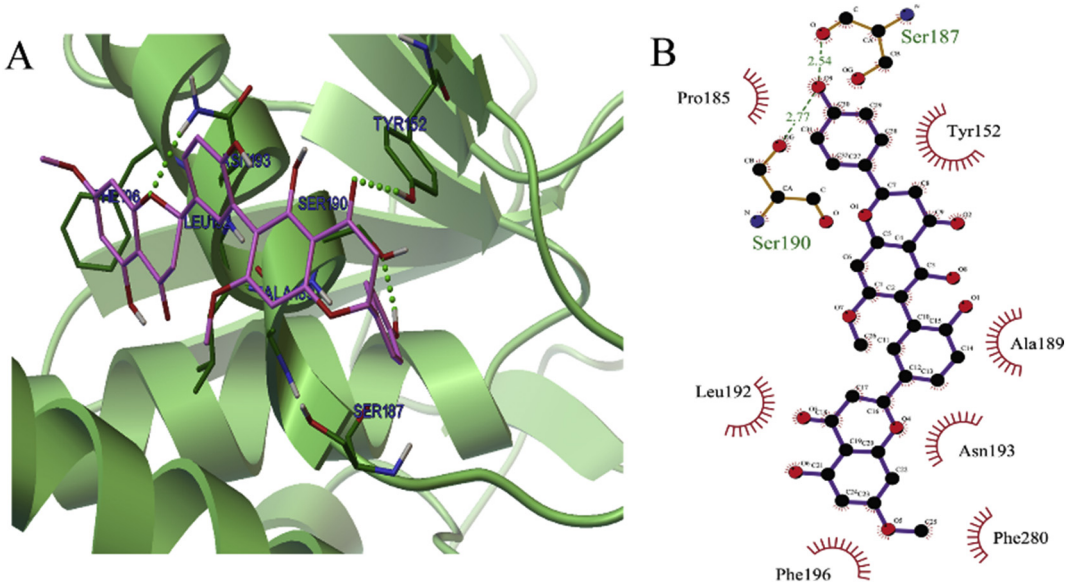

Fig. 3. Interaction of compound **1** with PTP1B (PDB ID: 1T49). (A) 3D docking molecule of PTP1B and compound **1**. (B) 2D ligand interaction diagram of PTP1B inhibition by compound **1**. Hydrogen bonding interactions are shown by green dashes. Carbons are in black and oxygens in red. (For interpretation of the references to colour in this figure legend, the reader is referred to the web version of this article.)

3.3. Molecular docking analysis

Molecular docking study is the application of computer based models to predict the conformation of ligand in the active site of particular receptor. To understand the possible mechanism of PTP1B inhibition and explain the difference of PTP1B activity between compounds **1–9**, the AutoDock Tools-1.5.6 program was used to analyze the molecular structures of PTP1B/inhibitor complexes. The docking score and binding residues are shown in Table 2. Take the new compound (**1**) for example, the PTP1B-compound **1** complex showed a − 7.16 kcal/mol binding energy with three hydrogen bonds of Ser187, Ser190 and Tyr152. The bond distances between **1** and the interacting amino acid residues were 2.54 Å for Ser187 and 2.77 Å for Ser190 (Fig. 3). In addition, several interacting residues of Ser187, Ala189, Leu192, Asn193 and Phe196 could also be observed. The residues Ser187 and Ala189 were involved in the helix α3, which could lead to allosteric inhibition of PTP1B activity [31]. The Leu192 and Phe196 were also two important residues for PTP1B allosteric inhibition. Compound **1** and the

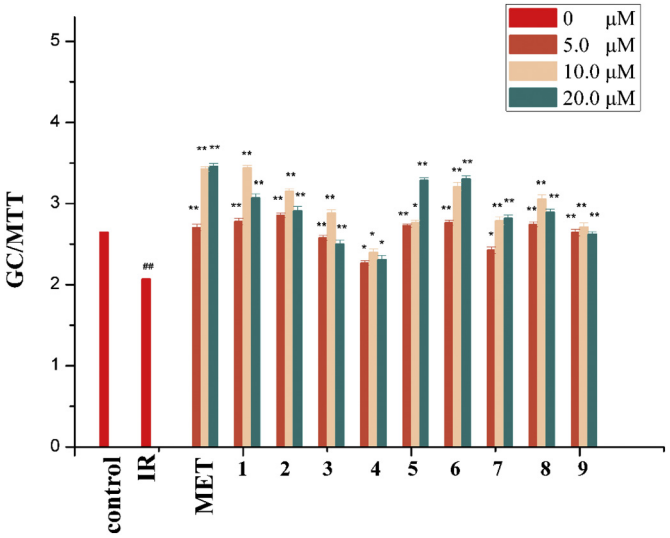

Fig. 4. Compounds **1–9** enhanced glucose uptake in insulin-resistant HepG2 cells at concentrations of 5, 10 and 20 μM. Data are presented as the mean ± SD of glucose uptake divided by the optical density determined in the MTT (n = 3). Met: metformin; IR: insulin-resistant HepG2 cells; $^{\#\#}p < 0.01$ versus control cells in the absence of insulin; * $p < 0.05$, ** $p < 0.01$ versus the control cells in the presence of insulin.

allosteric inhibitor shared the same binding residue Asn193 via hydrophobic interaction. The binding energies of compounds **2–9** were − 6.47, −6.02, −7.44, −8.88, −8.42, −7.72, −7.63, −9.49 kcal/mol, respectively, which revealed their high affinities on the binding sites of PTP1B (Table 2). The positive control ursolic acid exhibited a − 7.25 kcal/mol binding affinity to the allosteric site of PTP1B, with one hydrogen bond and interacting residues of Ser151, Tyr153, Ala189, Asn193, Phe280. These in silico results indicated that the isolates **1–9** were bound tightly at allosteric site of PTP1B, which were concordant with the results of in vitro enzyme activity assay.

3.4. Effect of the isolates on glucose uptake

Insulin is the most important hormone for the regulation of glucose metabolism. Defects in glucose uptake may decrease the sensitization of insulin and lead to insulin resistance. Liver is a key player for maintaining glucose homeostasis. HepG2 cells, the human hepatoma cells with phenotype similar to liver cells, are used as an ideal model of insulin resistance to mimic in vivo condition [32]. Therefore, we checked the effects of all the isolates on insulin-stimulated glucose uptake in insulin-resistant HepG2 cells. Firstly, the model of insulin-resistant in HepG2 cells was successfully established, which was evidenced by obvious decrease of glucose uptake in model cells compared to the control. The stimulatory abilities of **1–9** were further evaluated on glucose uptake in insulin-resistant HepG2 cells using a glucose kit. As show in Fig. 4, compounds **1–9** at concentrations of 5, 10 and 20 μM showed significant glucose consumption effect in insulin-resistant HepG2 cells, compared with the treatment of insulin. Especially, compound **1** exhibited the most potent glucose uptake stimulatory activity at the concentration of 10 μM. The cytotoxicity of **1–9** was evaluated by MTT assay, and the results showed that **1–9** had no cytotoxicity to HepG2 cells at a concentration of 20 μM after 24 h of incubation. Thus,

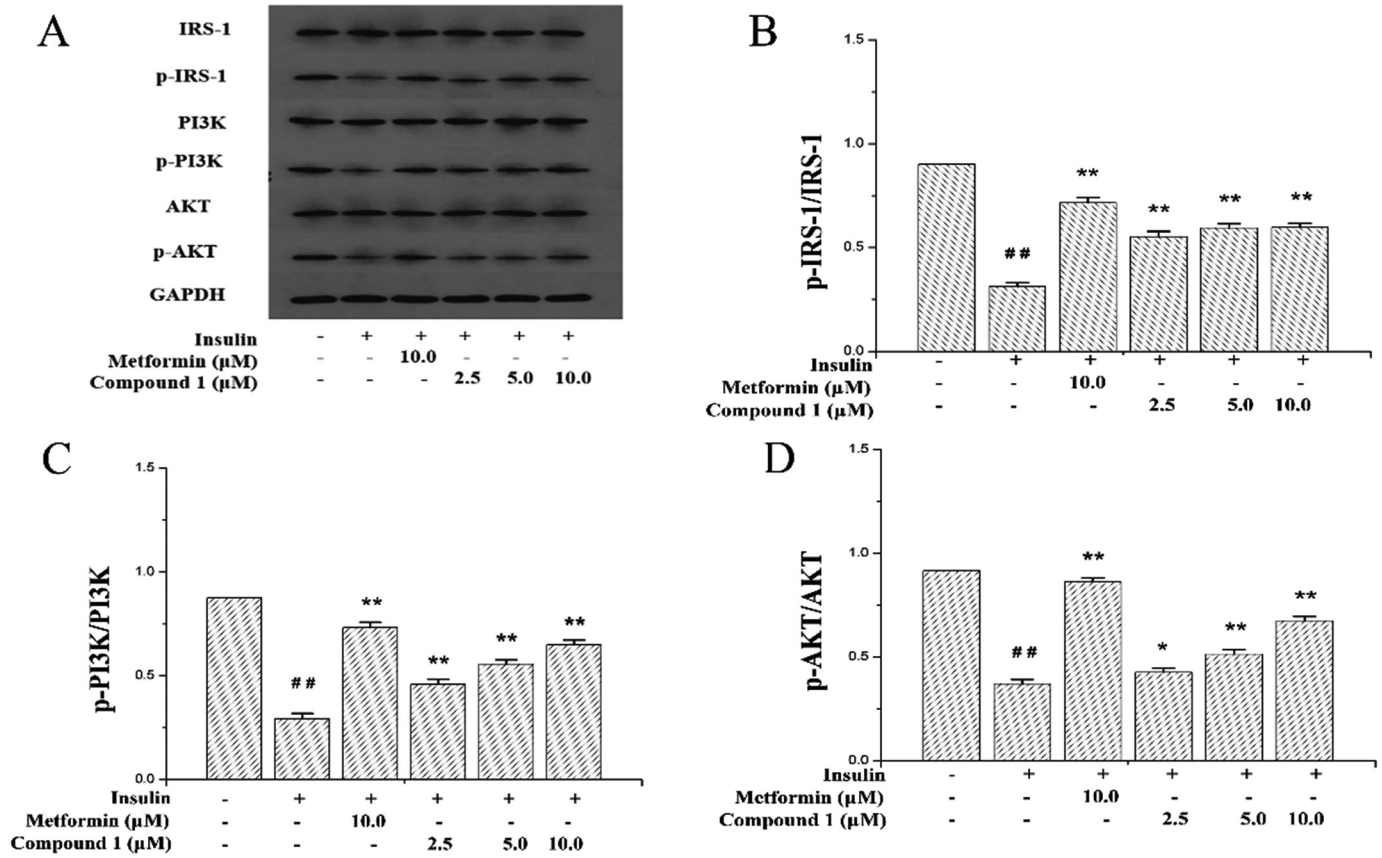

Fig. 5. Effect of compound **1** on insulin signaling pathway in insulin-resistant HepG2 cells. Cells were treated with 0, 2.5, 5.0, and 10.0 μM of compound **1** for the indicated times. (A) Exemplary western blot analyses of phosphorylated IRS-1, PI3K and Akt levels after treatment. Quantitative analyses on *p*IRS-1/IRS-1 (B), *p*PI3K/PI3K (C), and *p*AKT/AKT (D) were presented. $^{\#\#}p < 0.01$ versus control cells in the absence of insulin; * $p < 0.05$, ** $p < 0.01$ versus the control cells in the presence of insulin.

the stimulatory effects of **1–9** on glucose uptake were not affected by cytotoxicity, and the cell proliferation could be deducted by calculating the ratio of the GC and MTT. These results indicated that **1–9** from *S. uncinata* could promote glucose absorption in insulin-resistant HepG2 cells in vivo, and their effects may be related to but not limited to the inhibitory effects on the PTP1B enzyme.

3.5. Effects of compound 1 on the IRS-1/PI3K/AKT signaling pathway

To identify the mechanism underlying glucose uptake, the involvement of the insulin-mediated pathway was examined. The insulin mediated glucose uptake is initiated by activation of the insulin receptors (IRS). Among all IRS, IRS-1 is the predominant isoform and closely linked to glucose homeostasis in the liver. Phosphorylation of IRS-1 continues to activate downstream signaling, which involves phosphatidylinositol 3 kinase (PI3K) with the SH2 domain, as well as protein kinase B (Akt), an important target kinase downstream of this pathway. Activation of the IRS-1/PI3K/Akt pathway was determined following compound **1** treatment using western blotting. The concentration of **1** was chose as 2.5, 5, and 10 μM, since it exhibited the most potent glucose uptake stimulatory activity at the concentration of 10 μM. As shown in Fig. 5, compound **1** dose-dependently increased the expression of *p*-IRS-1, *p*-PI3K and *p*-Akt in insulin-resistant HepG2 cells, while did not affect the expression levels of total IRS-1, PI3K and Akt. These results suggested that **1** might contribute to enhancing glucose uptake through increasing the phosphorylation levels of IRS-1, PI3K and AKT, and further enhanced insulin sensitivity in insulin-resistant HepG2 cells.

4. Conclusion

In conclusion, the phytochemical investigations of the herb *S. uncinata* led to the isolation and structure elucidation of nine biflavonoids (**1–9**) including one previously unreported (**1**) and one with new configuration (**4**). These biflavonoids were classified into four types including robustaflavone-type, amentoflavone-type, delicaflavone-type and a C3′-O-C4‴ connected type. Their inhibitory activities against PTP1B were evaluated, and the structure-activity relationship was also discussed preliminary. The molecular docking simulation between PTP1B enzyme and biflavonoids supported the results. In addition, **1–9** significantly increased the glucose uptake in insulin-resistant HepG2 cells with **1** being the most potent one. Effect of **1** on the IRS-1/PI3K/Akt signaling pathway was also discussed. These results showed the potential of *S. uncinata* as a source of natural anti-diabetic agent.

Conflict of interests

The authors declare no conflict of interest.

Acknowledgements

This research was supported by the National Natural Science Foundation of China (31700306); Scientific and Technological Innovation Programs of Higher Education Institutions in Shanxi (201802065); and Shanxi Province Science Foundation for Youths (201701D221256).

Appendix A. Supplementary data

Supplementary data to this article can be found online at https://doi.org/10.1016/j.fitote.2019.104255.

References

[1] D.E. Moller, New drug targets for type 2 diabetes and the metabolic syndrome, Nature 414 (2001) 821–827, https://doi.org/10.1038/414821a.
[2] International Diabetic Federation (IDF), IDF Diabetic Atlas, 7th ed, (2016) http://www.vision2020uk.org.uk/idf-diabetes-atlas-7th-edition.
[3] A.R. Saltiel, New perspectives into the molecular pathogenesis and treatment of type 2 diabetes, Cell 104 (2001) 517–529, https://doi.org/10.1016/s0092-8674(01)00239-2.
[4] A.H. Mokdad, E.S. Ford, B.A. Bowman, W.H. Dietz, F. Vinicor, V.S. Bales, J.S. Marks, Prevalence of obesity, diabetes, and obesity-related health risk factors, 2001, JAMA 289 (2003) 76–79, https://doi.org/10.1001/jama.289.1.76.
[5] S. Zhang, Z.Y. Zhang, PTP1B as a drug target: recent developments in PTP1B inhibitor discovery, Drug Discov. Today 12 (2007) 373–381, https://doi.org/10.1016/j.drudis.2007.03.011.
[6] T.O. Johnson, J. Ermolieff, M.R. Jirousek, Protein tyrosine phosphatase 1B inhibitors for diabetes, Nat. Rev. Drug Discov. 1 (2002) 696–709, https://doi.org/10.1038/nrd895.
[7] M.T. Ha, D.H. Park, S. Shrestha, M. Kim, J.A. Kim, M.H. Woo, J.S. Choi, B.S. Min, PTP1B inhibitory activity and molecular docking analysis of stilbene derivatives from the rhizomes of *Rheum undulatum* L, Fitoterapia 131 (2018) 119–126, https://doi.org/10.1016/j.fitote.2018.10.020.
[8] J.H. He, L.X. Chen, H. Li, Progress in the discovery of naturally occurring anti-diabetic drugs and in the identification of their molecular targets, Fitoterapia 134 (2019) 270–289, https://doi.org/10.1016/j.fitote.2019.02.033.
[9] A. Vancura, P. Bu, M. Bhagwat, J. Zeng, I. Vancurova, Metformin as an anticancer agent, Trends Pharmacol. Sci. 39 (2018) 867–878, https://doi.org/10.1016/j.tips.2018.07.006.
[10] P.H. Nguyen, D.J. Jia, Y.R. Han, J.S. Choi, D.Y. Rhyu, B.S. Min, M.H. Woo, Selaginellin and biflavonoids as protein tyrosine phosphatase 1B inhibitors from *Selaginella tamariscina* and their glucose uptake stimulatory effects, Bioorg. Med. Chem. 23 (2015) 3730–3737, https://doi.org/10.1016/j.bmc.2015.04.007.
[11] H.P. Kim, H. Park, K.H. Son, H.W. Chang, S.S. Kang, Biochemical pharmacology of Biflavonoids: implications for anti-inflammatory action, Arch. Pharm. Res. 31 (2008) 265–273, https://doi.org/10.1007/s12272-001-1151-3.
[12] B. Yu, W. Cai, H.H. Zhang, Y.S. Zhong, J. Fang, W.Y. Zhang, L. Mo, L.C. Wang, C.H. Yu, *Selaginella uncinata* flavonoids ameliorated ovalbumin-induced airway inflammation in a rat model of asthma, J. Ethnopharmacol. 195 (2017) 71–80, https://doi.org/10.1016/j.jep.2016.11.049.
[13] D.H. Kim, P. Paudel, T. Yu, T.M. Ngo, J.A. Kim, H.A. Jung, T. Yokozawa, J.S. Choi, Characterization of the inhibitory activity of natural tanshinones from *Salvia miltiorrhiza* roots on protein tyrosine phosphatase 1B, Chem. Biol. Interact. 278 (2017) 65–73, https://doi.org/10.1016/j.cbi.2017.10.013.
[14] Z.Q. Liu, T. Liu, C. Chen, M.Y. Li, Z.Y. Wang, R.S. Chen, G.X. Wei, X.Y. Wang, D.Q. Luo, Fumosorinone, a novel PTP1B inhibitor, activates insulin signaling in insulin-resistance HepG2 cells and shows anti-diabetic effect in diabetic KKAy mice, Toxicol. Appl. Pharmacol. 285 (2015) 61–70, https://doi.org/10.1016/j.taap.2015.03.011.
[15] X. Hu, S. Wang, J. Xu, D.B. Wang, Y. Chen, G.Z. Yang, Triterpenoid Saponins from *Stauntonia chinensis* ameliorate insulin resistance via the AMP-activated protein kinase and IR/IRS-1/PI3K/Akt pathways in insulin-resistant HepG2 cells, Int. J. Mol. Sci. 15 (2014) 10446–10458, https://doi.org/10.3390/ijms150610446.
[16] P. Paudel, T. Yu, S.H. Seong, E.B. Kuk, H.A. Jung, J.S. Choi, Protein tyrosine phosphatase 1B inhibition and glucose uptake potentials of mulberrofuran G, albanol B, and kuwanon G from root bark of *Morus alba* L. in insulin-resistant HepG2 cells: an in vitro and in silico study, Int. J. Mol. Sci. 19 (2018) 1542–1560, https://doi.org/10.3390/ijms19051542.
[17] J.X. Zheng, N.L. Wang, H.W. Liu, H.F. Chen, M.M. Li, L.Y. Wu, M. Fane, X.S. Yao, Four new biflavonoids from *Selaginella uncinata* and their anti-anoxic effect, J. Asian Nat. Prod. Res. 10 (2008) 945–952, https://doi.org/10.1080/10286020802181166.
[18] D. Slade, D. Ferreira, J.P.J. Marais, Circular dichroism, a powerful tool for the assessment of absolute configuration of flavonoids, Phytochemistry 66 (2005) 2177–2215, https://doi.org/10.1016/j.phytochem.2005.02.002.
[19] J.X. Zheng, Y. Zheng, H. Zhi, Y. Dai, N.L. Wang, Y.X. Fang, Z.Y. Du, K. Zhang, M.M. Li, L.Y. Wu, M. Fan, New 3′,8″-linked biflavonoids from *Selaginella uncinata* displaying protective effect against anoxia, Molecules 16 (2011) 6206–6214, https://doi.org/10.3390/molecules16086206.
[20] M.L. Yi, X.F. Sheng, K.P. Xu, G.S. Tan, H. Zou, Flavonoids from *Selaginella uncinate*, Chin. J Chin. Mater. Med. 40 (2015) 3005–3008, https://doi.org/10.4268/cjcmm20151517.
[21] K. R. Markham, C. Sheppard, H. Geiger, ^{13}C NMR studies of some naturally occurring amentoflavone and hinokiflavone biflavonoids, Phytochemistry 26 (1987) 3335–3337, https://doi.org/10.1016/s0031-9422(00)82499-1.
[22] L.C. Lin, Y.C. Kuo, C.J. Chou, Cytotoxic biflavonoids from *Selaginella delicatula*, J. Nat. Prod. 63 (2000) 627–630, https://doi.org/10.1021/np990538m.
[23] Y.X. Zhang, Q.Y. Li, L.L. Yan, Y. Shi, Structural characterization and identification of biflavones in *Selaginella tamariscina* by liquid chromatography-diode-array detection/electrospray ionization tandem mass spectrometry, Rapid Commun. Mass Spectrom. 25 (2011) 2173–2186, https://doi.org/10.1002/rcm.5090.
[24] G.L. Silva, H. Chai, M.P. Gupta, N.R. Farnsworth, G.A. Cordell, J.M. Pezzuto, C.W.W. Beecher, A.D. Kinghorn, Cytotoxic biflavonoids from *Selaginella willdenowii*, Phytochemistry 40 (1995) 129–134, https://doi.org/10.1016/0031-9422(95)00212-P.
[25] P. Coulerie, M. Nour, A. Maciuk, C. Eydoux, J.C. Guillemot, N. Lebouvier, E. Hnawia, K. Leblanc, G. Lewin, B. Canard, B. Figadere, Structure-activity relationship study of biflavonoids on the dengue virus polymerase DENV-NS5 RdRp, Planta Med. 79 (2013) 1313–1318, https://doi.org/10.1055/s-0033-1350672.
[26] C.S. Ramalla, K. Olaf, S. Wolfgang, B. Franz, F. Daneel, S.R. Vanapatla, R.K. Bobbala, V.N.A.R. Achanta, Structurally unique biflavonoids from *Selaginella*

chrysocaulos and *Selaginella bryopteris*, Chem. Biodivers. 3 (2006) 404–414.
[27] L.C. Lin, C.J. Chou, Three new biflavonoids from *Selaginella delicatula*, Chin Pharm. J. 52 (2000) 211–218, https://doi.org/10.7019/CPJ.200008.0211.
[28] J.C. Xu, X.Q. Liu, K.L. Chen, A new biflavonoid from *Selaginella labordei* Hieron. ex Christ, Chin. Chem. Lett. 20 (2009) 939–941 (doi:10.10160.cclet.2009.03.046).
[29] C. Proençaa, M. Freitasa, D. Ribeiroa, J.L.C. Sousab, F. Carvalhoc, A.M.S. Silvab, P.A. Fernandesd, E. Fernandes, Inhibition of protein tyrosine phosphatase 1B by flavonoids: a structure-activity relationship study, Food Chem. Toxicol. 111 (2018) 474–481, https://doi.org/10.1016/j.fct.2017.11.039.
[30] T.H. Quang, N.T. Ngan, C.S. Yoon, K.H. Cho, D.G. Kang, H.S. Lee, Y.C. Kim, H. Oh, Protein tyrosine phosphatase 1B inhibitors from the roots of *Cudrania tricuspidata*, Molecules 20 (2015) 11173–11183, https://doi.org/10.3390/molecules200611173.
[31] C. Wiesmann, K.J. Barr, J. Kung, J. Zhu, D.A. Erlanson, W. Shen, B.J. Fahr, M. Zhong, L. Taylor, M. Randal, R.S. McDowell, S.K. Hansen, Allosteric inhibition of protein tyrosine phosphatase 1B, Nat. Struct. Mol. Biol. 11 (2004) 730–737, https://doi.org/10.1038/nsmb803.
[32] D. Gupta, S. Varma, R.L. Khandelwal, Long-term effects of tumor necrosis factor-alpha treatment on insulin signaling pathway in HepG2 cells and HepG2 cells overexpressing constitutively active Akt/PKB, J. Cell. Biochem. 100 (2007) 593–607, https://doi.org/10.1002/jcb.21080.